Original

Effect of type and amount of alumina as dopant over the densification and the electrical properties of zinc oxide ceramic electrodes

M.-J. Sánchez-Rivera [a,*], M.J. Orts [a,b], V. Pérez-Herranz [c], S. Mestre [a,b]

[a] University Institute of Ceramic Technology (IUTC), Jaume I University, Castellón, Spain
[b] Department of Chemical Engineering, Jaume I University, Castellón, Spain
[c] IEC Group, ISIRYM, Universitat Politècnica de València, València, Spain

A R T I C L E   I N F O

A B S T R A C T

Aluminum-doped zinc oxide (AZO) electrodes can be a good alternative to replace the expensive electrodes (Ti, ITO, FTO, etc.), which are used in the electrooxidation process to remove refractory and emergent contaminants from industrial wastewaters. AZO electrodes have been prepared by the traditional ceramic method using ZnO as the main raw material and different precursors of Al_2O_3 as dopant sources. Densification, microstructure and electric resistivity of AZO electrodes are a function of precursor's nature and sintering thermal treatment. The higher the number of precursor's particles and the smaller their size, the sintering temperature needed to attain high densifications and low resistivities shifted to higher values. Micrometric and colloidal alumina were the precursors which allowed to equilibrate an affordable sintering temperature interval (1200–1300 °C) with acceptable densification and resistivity values (around 95% and 5×10^{-3} Ω cm, respectively). However, colloidal alumina made it possible to obtain slightly lower values of resistivity at the cost of having a narrower working interval.

Efecto del tipo y cantidad de alúmina como dopante sobre la densificación y las propiedades eléctricas de electrodos cerámicos de óxido de zinc

R E S U M E N

En este trabajo de investigación se presentan electrodos cerámicos de óxido de zinc dopado con aluminio (AZO) como alternativa a los actuales electrodos de titanio (ITO, FTO…) utilizados en el proceso de electrooxidación de aguas residuales para la eliminación de contaminantes refractarios y emergentes. Estos electrodos AZO han sido preparados mediante el método tradicional cerámico, utilizando ZnO como materia prima principal y diferentes precursores de Al_2O_3 como dopantes. La densificación, la microestructura y la resistividad

* Corresponding author.
  E-mail address: mariajose.sanchez@itc.uji.es (M.-J. Sánchez-Rivera).

eléctrica de estos electrodos son propiedades que están directamente relacionadas con la naturaleza del precursor y con el tratamiento térmico utilizado para su sinterización. Cuanto mayor es el número de partículas del precursor y menor es su tamaño, la temperatura de sinterización necesaria para lograr altas densificaciones y bajas resistividades cambia a valores más altos. Fueron la alúmina micrométrica y la coloidal los dopantes que ofrecieron un buen equilibrio entre temperatura de sinterización (1.200–1.300 °C) y densificación-resistividad (95% y 5·10^{-3} Ω cm, respectivamente). Concretamente en el caso de la alúmina coloidal, se pudieron optimizar estos resultados estrechando el intervalo de temperatura de trabajo.

Introduction

In recent years, there has been an increasing concern about the elimination of recalcitrant or emergent organic compounds present in industrial wastewaters. One of the most promising methods to eliminate these compounds is the electrooxidation [1]. In this process, electrochemically generated hydroxyl radicals mineralize organic compounds. Therefore, it is necessary the use of electrodes which facilitate the generation of hydroxyl radicals and, at the same time, withstand the highly oxidizing medium. This double requirement has been met with expensive materials, either because they contain scarce elements (Pt, Ti, In, etc.), or because they require sophisticated processing techniques (Ti covered with boron-doped diamond), [2,3]. In addition to metallic electrodes (Pt, Ti), ceramic electrodes have also been used as sub-stoichiometric titanium oxides (TiO$_{2-x}$), tin-doped indium oxide (ITO) or tin oxide doped with fluorine (FTO) [4,5].

Zinc oxide is a semiconductor material used in numerous applications given its wide range of physical–chemical properties. Some of the most known ones are optoelectronic devices, piezoelectric nanogenerators, thin film electrodes, light emitting devices or ceramics with a sustainable antibacterial activity [6–11]. Many studies have determined that the electrical and optical properties of ZnO are controlled by impurities and defects present in its structure. Group III elements as Al, Ga, and In, are well-known donor dopants in ZnO. Concretely, Al(III) allows to maintain the hexagonal wurtzite structure of zinc oxide while helping to improve its properties [12–14]. Consequently, mixtures Al$_2$O$_3$ + ZnO allow to synthesize ceramic electrodes in relatively affordable processing conditions. A good example are the sputtering targets of (Al,Zn)O synthesized by simultaneous reaction and sintering of a blend 95 wt.% ZnO and 5 wt.% Al$_2$O$_3$, which also present a low electrical resistivity (0.1 Ω cm) [15–19].

In the studies carried out so far, different techniques were employed for the synthesis of Al-doped ZnO electrodes such as chemical co-precipitation, sputtering or sol-gel processing. However, the traditional ceramic method could be optimized in order to synthesize electrodes with good performance. Concretely, a successful choice of the aluminum oxide precursor and the thermal treatment could allow the manufacture of electrodes with a good cost/performance relation. In this work, the effects of the aluminum oxide precursor and the parameters of the thermal treatment on the sintering behavior and the properties of the electrodes obtained throughout the traditional ceramic method were investigated. Firstly, the effects of four aluminum oxide precursors were compared with an Al-free reference. Secondly, the effects of thermal treatment parameters for the two more favorable precursors were evaluated by means of a 2^5 factorial experimental design, as described by Box et al. [20]. Finally, it was investigated whether resistivity and densification were relatively stable around the minimum identified in the design of experiments. That is, if small variations in operating conditions did not cause an unacceptable change in these properties.

Experimental procedure

Electrode's main raw material was ZnO (purity 98%, Panreac Quimica SLU, Spain). Four different aluminum oxide precursors were selected: micrometric Al$_2$O$_3$ (AR12-B5, Pechiney SA, France), nanometric Al$_2$O$_3$ (Aeroxide®, Evonik, Germany), Al$_2$O$_3$ colloidal dispersion (20% in H$_2$O, Alfa Aesar, Germany) and Al(NO$_3$)$_3$·9H$_2$O (98–102%, Panreac, Spain). Polyvinylalcohol (Mowiol 4-88, Sigma Aldrich, Germany), was added to each composition as a ligand (0.8 wt.%).

The preparation of the electrodes was carried out through the traditional ceramic method, adapting the method employed in previous research [21]. Firstly, the raw materials were mixed during an hour in a planetary mill (Pulverisette 5, Fritsch GmbH, Germany), at 230 rpm using water as a fluid. Secondly, suspensions were dried at 110 °C for 24 h, then the resulting powder was sieved through a 600 μm mesh and moistened to 5.0% (kg water/kg dry solid). Thirdly, prismatic specimens of 1.0 cm thickness, 1.0 cm width and 4.0 cm length were dry-pressed at 450 kg cm^{-2} in a laboratory uniaxial press (Casmon S.A., Spain) and dried in an oven at 110 °C. Finally, the test specimens were sintered in a laboratory furnace (RHF1600, Carbolite Furnaces, UK).

Bulk density of green and sintered ceramic bodies was measured by Archimedes' method. The densification was calculated according to German [22] as the change in bulk density due to sintering divided by the change needed to obtain a pore-free solid. Resistivity was measured with a resistance meter HIOKI RM 3545, averaging ten measurements in each specimen. The microstructure was analyzed by FEG-SEM (QUANTA 200F, FEI Co., USA) from polished sections of selected specimens, which in some cases were thermally etched before the analysis.

In the first series of experiments, all compositions were calculated to maintain a 98.5/1.5 ZnO/Al$_2$O$_3$ molar ratio in

**Table 1 – Compositions used in the first series of experiments.**

Reference	ZnO (mol.%)	Aluminum precursor	
		Type	mol.%
M	98.50	Micro-Al$_2$O$_3$	1.50
N	98.50	Nano-Al$_2$O$_3$	1.50
C	98.50	Colloidal-Al$_2$O$_3$	1.50
H	97.04	Aluminum nitrate	2.96
R	100	–	–

Table 3 – Experimental design for the third series of experiments.

Level	Colloidal-Al$_2$O$_3$ (mol.%)	Soaking time (h)
−1	0.5	1
0	1.0	3
1	1.5	6

Fig. 1 – Evolution with T_{max} of the sintering weight loss of the specimens of the five compositions.

the sintered specimens, except the aluminum-free composition which was used as a reference (Table 1). Some variations were introduced in the mixing step for compositions C and H. In the case of the mixture with colloidal alumina (composition C), the pH of the water was equalized to that of the colloidal dispersion by a small addition of nitric acid in order to avoid colloid's gelation. In the case of the composition with aluminum nitrate (composition H), 20 mL of ammonia were added after mixing to precipitate aluminum hydroxide and the suspension was mixed again for 10 min with the objective was to generate small and well dispersed particles of aluminum hydroxide. SEM analysis of the mixture confirmed the high degree of homogeneity (not shown). The sintering was performed with a thermal treatment designed in previous experiments, characterized by a heating rate of 15 °C min^{-1} up to maximum temperature (T_{max}), then a dwell time of 6 h at T_{max} and finally a natural cooling. Different maximum temperatures were evaluated for every composition between 1100 °C and 1350 °C. An exception was composition H, which was sintered with a heat treatment characterized by additional steps at low temperature (up to 500 °C) to avoid the breakage of the specimens under the pressure of the gases released by some compounds present as result of the reaction between ammonia and aluminum nitrate (see experimental results section). However, these changes did not modify the high temperature section of the cycle (final heating rate and soaking time at T_{max}). Two of the alumina precursors were selected for next stage.

In the second part of this work, and using the same experimental procedure described above, the 2^5 design of experiments described in Table 2 was carried out (according to Box et al. [20]). The effects of the five variables were evaluated and, as a result, the most favorable Al$_2$O$_3$ precursor was selected. Finally, additional experiments with the selected alumina precursor were carried out, modifying precursor's proportion and soaking time, to analyze the stability of the resistivity and densification around the optimum identified in the previous stage (Table 3).
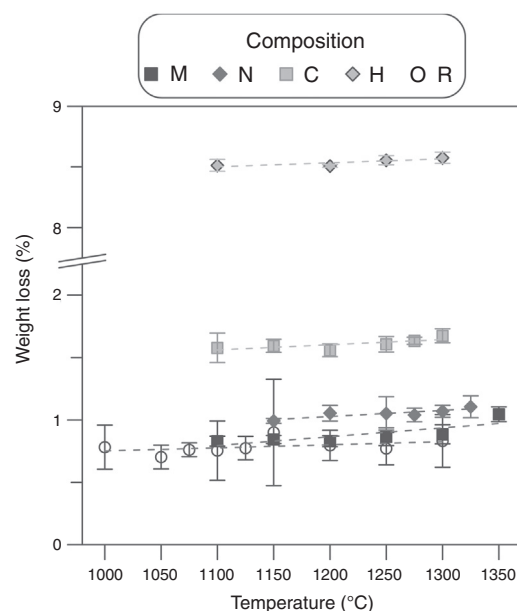
Experimental results and discussion

Weigh loss evolution as a function of T_{max} and Al$_2$O$_3$-precursor (Fig. 1) showed a subtle effect of the first variable and a noticeable effect of the second one. The five compositions slightly increased the weight loss as sintering temperature increased, pointing to a very small rate of volatilization of ZnO in the studied interval (the mean of the slopes was 0.0004 wt.% °C^{-1}). Considering that the Al-free composition showed a weight loss practically equal to the PVA's proportion in every composition (0.8 wt.%), the main effect over weight loss was due to alumina precursors. Micrometric alumina barely modified weight loss, but nanometric and colloidal alumina provoked slight increases, probably due to different amounts of adsorbed water. The strongest effect was showed by composition H, whose thermogravimetric analysis showed three thermal losses in the 25–150 °C, 150–223 °C and

Table 2 – Factorial experimental design 2^5. Two levels for 5 variables: aluminum precursor, proportion, heating rate, maximum temperature and soaking time (coded as A, %, r, T and t, respectively).

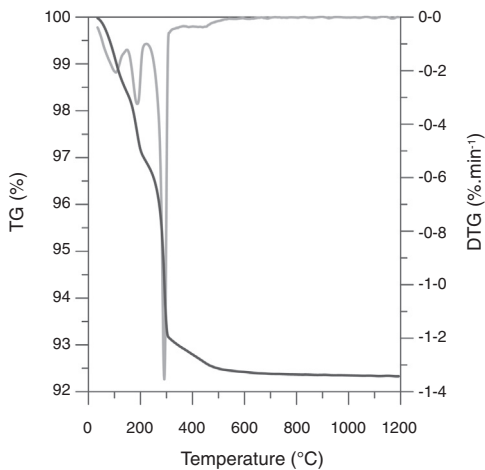| Level	Aluminum precursor	Proportion (mol.%)	Heating rate (°C min^{-1})	T_{max} (°C)	Soaking time (h)
−1	Micro-AlO$_3$	1	5	1200	1
+1	Colloidal-Al$_2$O$_3$	3	15	1300	6

Fig. 2 – **Thermogravimetric analysis of composition H.**
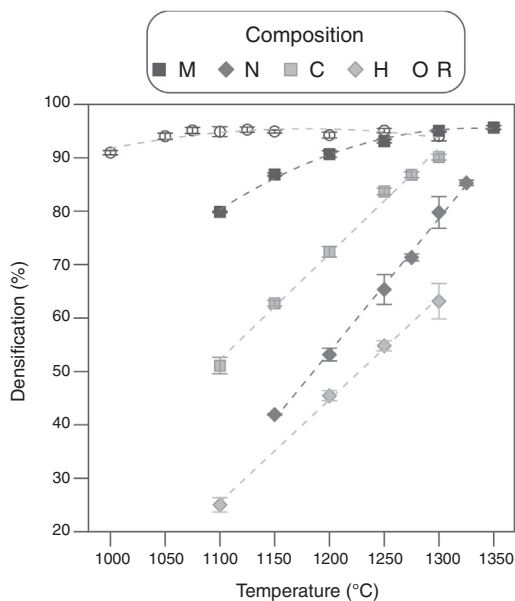
Fig. 3 – **Evolution with T_max of the densification of the specimens of the five compositions.**
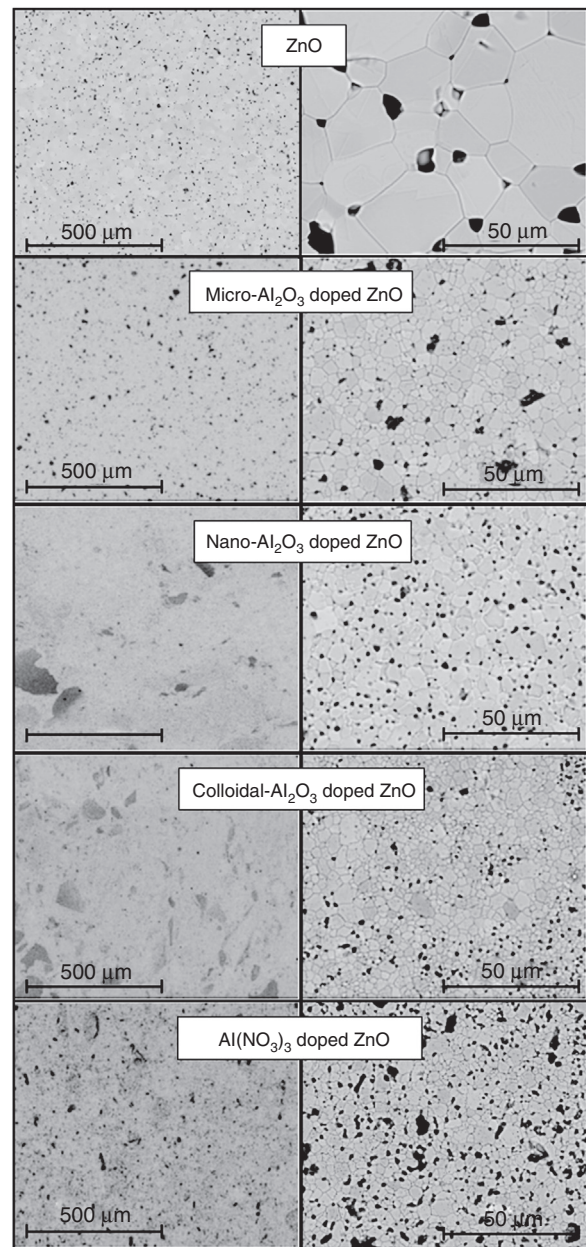

Fig. 4 – **Microstructure of polished sections of the specimens of the five compositions, which had reached the maximum densification in the explored temperature interval.**

223–500 °C intervals (Fig. 2). The first loss could be assigned to adsorbed water, the second to ammonium nitrate volatilization (boiling point of pure NH_4NO_3 is 210 °C according to Chaturvedi et al. [23]) and the third to aluminum hydroxide decomposition according to Temuujin et al. [24]. That gas releases justified the change in the thermal treatment for sintering composition H specimens.

The effect of the alumina precursor was also noticed in the densification, but temperature had similarly a strong effect over this parameter (Fig. 3). The Al-free composition (R) densified nearly completely in the 1100–1250 °C interval, showing a slightly parabolic trend. This high densification was reflected in the microstructure (Fig. 4), which is characteristic of the last stage of sintering (large grains and some isolated pores). The effect of Al_2O_3 addition can be described in broad lines as a combination of a shift of the parabola to higher temperatures

and an increase in their curvature. Consequently, the low temperature branch approaches a straight line, and the maximum densification is displaced out of the explored T_{max} interval. Micrometric Al_2O_3 had the lowest effect (composition M), as it shifted the temperature of maximum densification to 1350 °C and increased the slope of the densification–temperature curve. This change was reflected in the mixture of large and small pores, which is the characteristic of its microstructure. In addition, the grains were smaller than the ones of Al-free composition, but the alumina particles were not clearly distinguished. Colloidal Al_2O_3, nanometric Al_2O_3 and aluminum
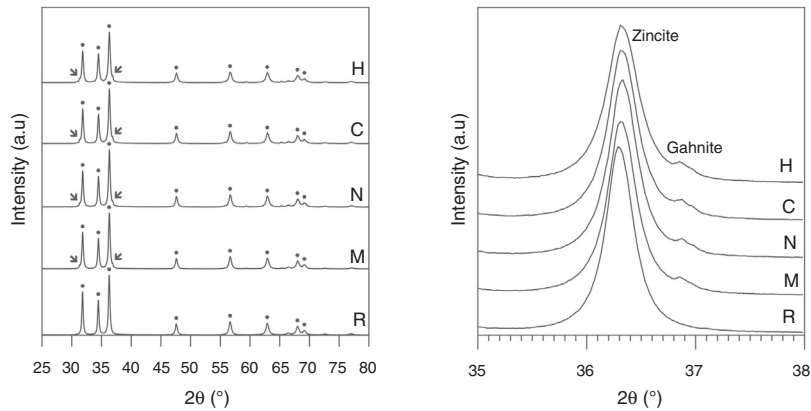
Fig. 5 – X-ray diffraction of the sintered specimens of the five compositions.

hydroxide, in this order, displaced progressively the curve toward lower densifications in the explored interval.

Specimens' microstructures changed in parallel. Instead of large rounded pores, there were a lot of small pores, but their mean size increased, and the grain size decreased, as colloidal Al_2O_3 was substituted by nanometric Al_2O_3 or aluminum hydroxide. In addition, it also seemed that aluminum hydroxide provoked some defects along the dry-pressing step. Obviously, the addition of Al_2O_3 precursors delays sintering, but its size and degree of dispersion modulates the effect. Colloidal alumina and nanometric alumina were expected to provoke the most noticeable effects, but their dispersion was not perfect as showed the SEM images. Both precursors tend to form agglomerates that survive the mixing process (darker areas in the SEM images). By the contrary, aluminum hydroxide mixes better and, consequently, their effect over densification is the strongest.

X-ray diffraction of the specimens sintered at 1300 °C showed that the main phase was zincite (wurtzite-type ZnO) in all the samples (Fig. 5, left). There is also a small proportion of gahnite (spinel-type $ZnAl_2O_4$) in the Al-containing specimens as a secondary phase, but no signal of free aluminum oxide. In addition, the reflections of zincite show a slight displacement in the Al-containing specimens with respect to the Al-free reference (Fig. 5, right), which is a hint of the solid solution formation. The proportions of spinel or solid solution are very small, so they are difficult to measure with precision, but the similarity in the area of the spinel reflections suggest that the aluminum precursor reacts quickly with ZnO to generate spinel, independently of the nature of Al precursor. However, spinel formation is a slower process, which cannot end in the time used in experiments.

Alumina precursor also had a strong effect over electrical resistivity (ρ), as it changed completely the shape and location of the curve $\rho = f(T_{max})$ of ZnO (Fig. 6). Resistivity of the sintered specimens of undoped zinc oxide showed a not very pronounced minimum around 1050 °C ($\approx 2\,\Omega\,cm$), while resistivity values are maintained within a range of approximately one order of magnitude. Theoretically, Al doping must reduce the resistivity's values by the formation of Al_2O_3–ZnO solid solution. However, the actual effect depended on the type of precursor, since, as visualized in the microstructures,
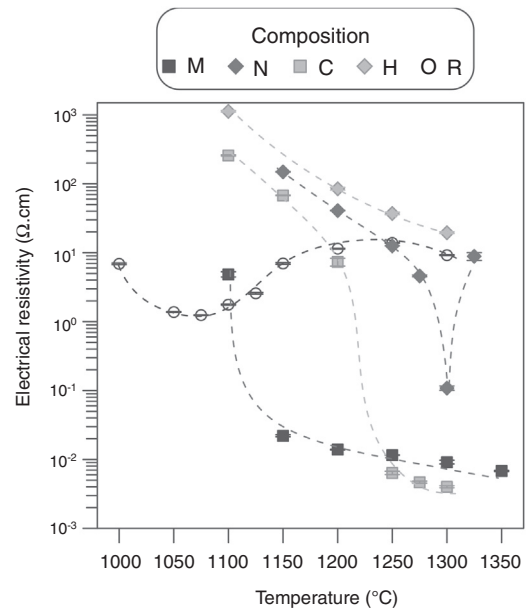

Fig. 6 – Evolution with sintering temperature of the electrical conductivity of the specimens of the five compositions.

each one interacted differently with ZnO. The analysis of the $\rho = f(T_{max})$ curves and the microstructures allowed to formulate a hypothesis about the effect of Al_2O_3 precursor. In the low sintering temperature interval, the effect of alumina precursor was a reduction of densification by one hand, and a negligible formation of the solid solution by the other. As a result, the resistivity was higher than the one corresponding to undoped ZnO sintered at the same T_{max}, which was more densified. At some sintering temperature, a continuous path of solid solution was formed as a result of the combination of higher densification and solid solution formation, which leaded to a significant reduction in resistivity (about two orders of magnitude, reaching values around $1 \times 10^{-2}\,\Omega\,cm$). For higher sintering temperatures, the resistivity decreased a little more as a higher proportion of solid solution was formed, although the densification did not increase greatly.

Obviously, the critical temperature was different for every Al_2O_3 precursor tested. In the case of micrometric alumina this temperature was around 1150 °C, 1250 °C for colloidal alumina and 1300 °C for nanometric alumina. This critical point was not attained for aluminum hydroxide in the explored T_{max} interval. However, it was estimated to be higher than 1400 °C by extrapolation of the densification $=f(T_{max})$ function, considering that the three critical temperatures obtained corresponded to densifications around 80%. According to this hypothesis, the lower resistivity value obtained with colloidal alumina with respect to micrometric alumina at 1300 °C was due to a higher proportion of solid solution, favored by the higher reactivity of colloidal particles, as its densification is slightly lower. The behavior of composition N deviated from the hypothesis, as there was a sharp increase in resistivity after the critical point (this experiment was replicated to confirm the unexpected result). An explanation could be proposed from the microstructure of composition N's specimens, in which nanoparticles formed agglomerates and were not fully dispersed. Firstly, there was an incipient formation of the solid solution at T_{max} 1300 °C, which reduced the resistivity. Secondly, a layer of insulating spinel ($ZnAl_2O_4$) could have been formed in the alumina-zinc oxide interphase at higher temperatures, with increased the resistivity up to the values of the undoped zinc oxide, because this material would be the only path for electron transfer.

Considering the previous results, an acceptable compromise was needed between sintering temperature and the precursor of alumina to obtain specimens with low resistivity and high densification. In this sense, compositions M and C managed to improve the Al-free composition's resistivity (reaching values close to 10^{-3} Ω cm), without reducing densification too much, and employing an affordable T_{max} interval (1200–1300 °C). Consequently, compositions M and C were selected as a basis for a 2^5 factorial experimental design intended for selecting the most suitable precursor, as well as the operating parameters with the greatest effect on densification and resistivity. In addition to Al_2O_3 precursor and T_{max}, the precursor's proportion, heating rate and soaking time effects, were also investigated (Table 2).

Results showed that micrometric alumina's addition led to a more robust response, specially at the lowest proportion, as densification and resistivity had a low dependence on thermal treatment's parameters (Figs. 7 and 8). The highest proportion of micrometric alumina allowed a small improvement in resistivity, but with the counterpart of more energetic thermal cycles and a reduction in densification. In the case of colloidal alumina (composition C), densification and resistivity were very sensitive to its proportion, as well as to the parameters of sintering's thermal cycle, being system's response clearly less robust. However, it was possible to obtain densifications and resistivities of the same order as the best values obtained with micrometric alumina under certain conditions (lowest proportion of colloid and thermal cycles characterized by high values of T_{max}).

The calculation of the main effects and their interactions, and the evaluation of their significance by ANOVA test (according to Box et al. [17], Figs. 9 and 10), showed that the precursor (A), its proportion (%) and sintering temperature (T) were the significant main effects for densification and resistivity (in the
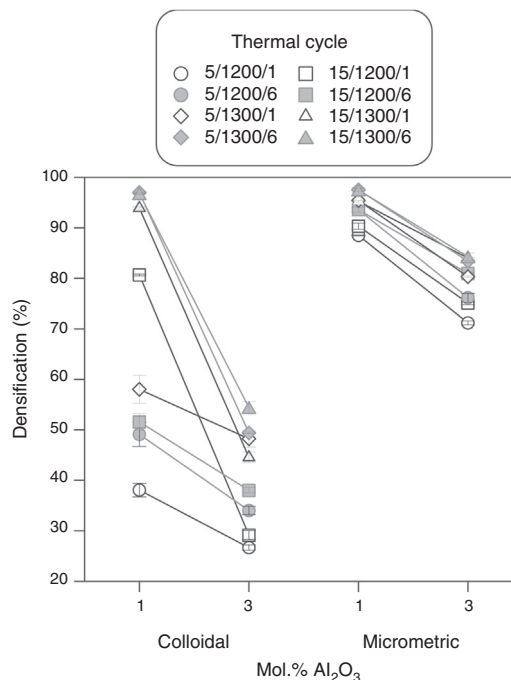

Fig. 7 – Specimen' densification as a function of the percentage of alumina (colloidal or micrometric) and thermal cycle parameters (heating rate/T_{max}/soaking time).
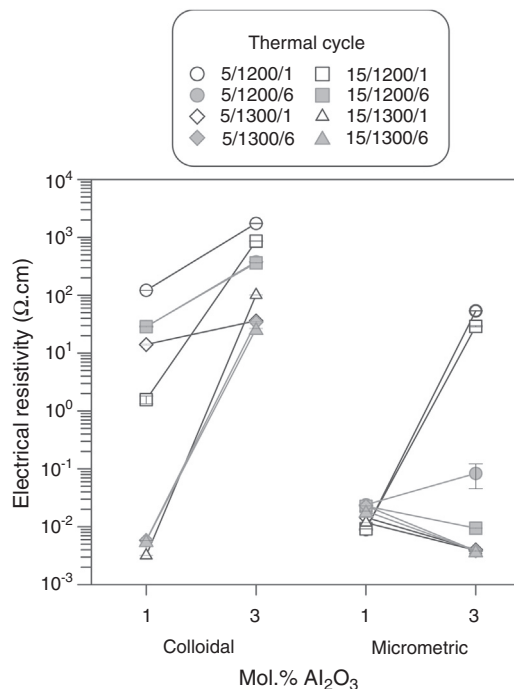

Fig. 8 – Specimens' electrical resistivity as a function of the percentage of alumina (colloidal or micrometric) and thermal cycle parameters (heating rate/T_{max}/soaking time).

case of this last property, the main effects and interactions were calculated with the logarithm of its value, given the broad interval of variation that it presented [15]). In the case of interactions, A × % interaction (alumina precursor × proportion of
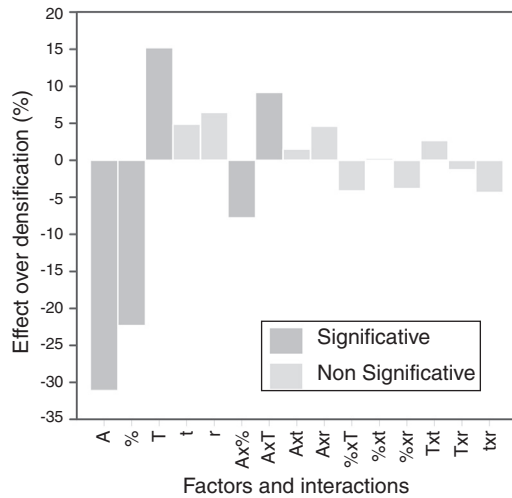
Fig. 9 – Calculated effects over densification of the five variables of the 2^5 experimental design.
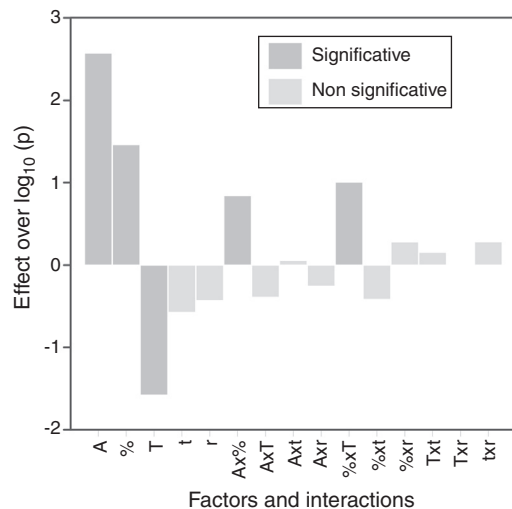

Fig. 10 – Calculated effects over electrical resistivity of the five variables of the 2^5 experimental design.

precursor) was significant for densification and resistivity, $A \times T$ interaction (alumina precursor $\times T_{max}$) was only significant for densification and $\% \times T$ interaction (proportion of precursor $\times T_{max}$) was only significant for resistivity. Heating rate (r) and soaking time (t) were not significant main factors according to these results and they did not participate in any significant interaction either. These results confirm in broad lines that a huge number of alumina particles were detrimental for densification and resistivity (a finer alumina and in greater proportion), and a higher sintering temperature could reduce resistivity by favoring the formation of the solid solution.

From the analysis of the previous data it was concluded that the electrodes with better performance were those which have been synthesized at 1300 °C with a heating rate of 15 °C min^{-1}, being doubtful if the soaking time at maximum temperature could be reduced to 1 hour. Both precursors (micrometric alumina and colloidal alumina) generated specimens of low resistivity and almost equal densification values
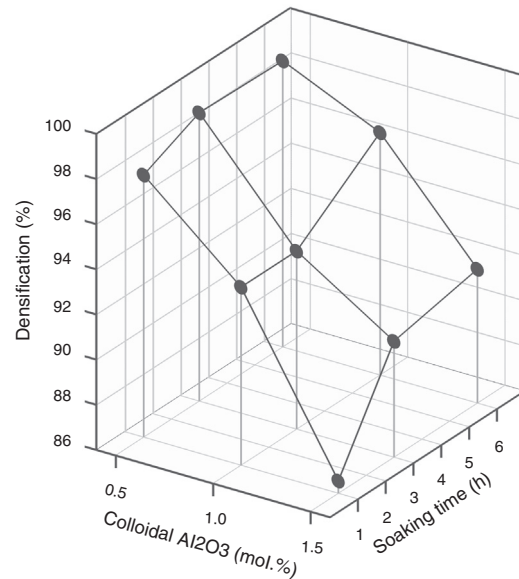

Fig. 11 – Densification's evolution of the specimens as a function of soaking time and proportion of colloidal alumina.

when their content was 1.0 mol.%. However, the composition with 1.0 mol.% of colloidal alumina had a slightly lower resistivity than composition with 1.0 mol.% micrometric alumina, but, apparently, their properties were more sensitive to changes in thermal treatment's parameters.

Since colloidal alumina allowed to attain lower values of resistivity but with greater influence of process parameters, it was considered convenient to analyze whether there was a sufficiently wide operating interval. A response surface methodology was applied, taking as variables the percentage of colloidal alumina and the soaking time (Table 3), fixing the heating rate in 15 °C min^{-1} and the maximum temperature in 1300 °C. Results indicated that there was an interval of colloidal alumina content and residence time within which the lowest resistivity values are achieved (1.0–1.5 mol.% and 1–3 h, Fig. 11). However, the densification does not present such a minimum, but instead presents a decreasing tendency as the amount of colloidal alumina increases, more pronounced the shorter the residence time (Fig. 12). Considering that data obtained with 3 mol.% of colloidal alumina and similar heat treatments (Fig. 7) corresponded to higher resistivities and noticeably lower densifications, it was evident that increasing the proportion of colloidal alumina would not improve the desired characteristics. Synthesis conditions must reach a compromise between low resistivity and high densification, which obviously corresponds to colloidal alumina proportions around 1.0 mol.% and residence times at 1300 °C around 3 hours. Outside this interval, at least one of the properties takes inappropriate values.

Conclusions

It was possible to synthesize ceramic electrodes based in aluminum doped zinc oxide by the ceramic method, without using any special technique for shaping of the electrodes or
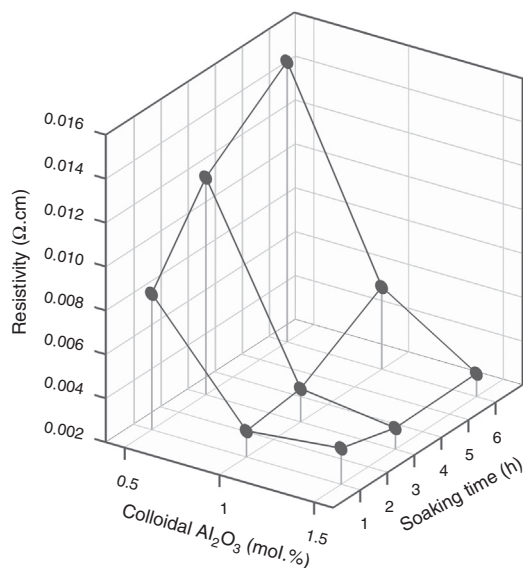
Fig. 12 – Electrical resistivity's evolution of the specimens as a function of soaking time and proportion of colloidal alumina.

for their sintering. The aluminum precursor and the maximum temperature of the heat treatment mainly conditioned the densification and resistivity of the sintered electrode. The temperature of maximum densification was shifted to higher values the higher the number of alumina particles incorporated and the smaller their size (from 1100 °C of pure ZnO to around 1400 °C for some alumina precursor). Doping with alumina reduced sintered ZnO's resistivity when enough proportion of Al_2O_3-ZnO solid solution had been formed. The experiments suggested that this point was reached for densifications higher than 80%, but the interaction between ZnO and Al_2O_3 depended on the alumina precursor's size of particle or agglomerate. Consequently, the type of aluminum precursor conditioned the resistivity and densification of ZnO. Between the four precursors tested, micrometric alumina and colloidal alumina were the ones that allowed a better balance between resistivity and densification, employing thermal treatments characterized by affordable maximum temperatures. Colloidal alumina allowed slightly lower resistivity values to be achieved at the cost of a narrower range of operating conditions than micrometric alumina, but still large enough for the results to be sufficiently reproducible.

Acknowledgements

R E F E R E N C E S

[1] J.A. Barrios, E. Becerril, C. De León, C. Barrera-Díaz, B. Jiménez, Electrooxidation treatment for removal of emerging pollutants in wastewater sludge, Fuel 149 (2015) 26–33, http://dx.doi.org/10.1016/j.fuel.2014.10.055.

[2] C.A. Martínez-Huitle, S. Ferro, Electrochemical oxidation of organic pollutants for the wastewater treatment: direct and indirect processes, Chem. Soc. Rev. 35 (2006) 1324–1340, http://dx.doi.org/10.1039/B517632H.

[3] C.A. Kent, J.J. Concepcion, C.J. Dares, D.A. Torelli, A.J. Rieth, A.S. Miller, P.G. Hoertz, T.J. Meyer, Water oxidation and oxygen monitoring by cobalt-modified fluorine-doped tin oxide electrodes, J. Am. Chem. Soc. 135 (2013) 8432–8435, http://dx.doi.org/10.1021/ja400616a.

[4] H. Kim, R.C.Y. Auyeung, A. Piqué, Transparent conducting F-doped SnO_2 thin films grown by pulsed laser deposition, Thin Solid Films 516 (2008) 5052–5056, http://dx.doi.org/10.1016/j.tsf.2007.11.079.

[5] K. Aijo John, R.R. Philip, P. Sajan, T. Manju, In situ crystallization of highly conducting and transparent ITO thin films deposited by RF magnetron sputtering, Vacuum 132 (2016) 91–94, http://dx.doi.org/10.1016/j.vacuum.2016.07.035.

[6] C. Klingshirn, ZnO: from basics towards applications, Phys. Status Solidi Basic Res. 244 (2007) 3027–3073, http://dx.doi.org/10.1002/pssb.200743072.

[7] J.S. Liu, C.X. Shan, H. Shen, B.H. Li, Z.Z. Zhang, et al., ZnO light-emitting devices with a lifetime of 6.8 hours, Appl. Phys. Lett. 101 (2012) 011106, http://dx.doi.org/10.1063/1.4733298.

[8] A.K. Sood, Z. Wang, D.L. Polla, N.K. Dhar, T. Manzur, A.F.M. Anwar, ZnO nanostructures for optoelectronic applications, in: O. Sergiyenko (Ed.), Optoelectronic Devices and Properties, InTechOpen Ltd., London, 2011, http://dx.doi.org/10.5772/618.

[9] Z.L. Wang, J. Song, Piezoelectric nanogenerators based on zinc oxide nanowire arrays, Science 312 (5571) (2006) 242–246, http://dx.doi.org/10.1126/science.1124005.

[10] H. ming Zhou, D. qing Yi, Z. ming Yu, L. rong Xiao, J. Li, Preparation of aluminium doped zinc oxide films and the study of their microstructure, electrical and optical properties, Thin Solid Films 515 (2007) 6909–6914, http://dx.doi.org/10.1016/j.tsf.2007.01.041.

[11] K. Hirota, M. Sugimoto, M. Kato, K. Tsukagoshi, T. Tanigawa, H. Sugimoto, Preparation of zinc oxide ceramics with a sustainable antibacterial activity under dark conditions, Ceram. Int. 36 (2010) 497–506, http://dx.doi.org/10.1016/j.ceramint.2009.09.026.

[12] D.C. Look, Progress in ZnO materials and devices, J. Electron. Mater. 35 (2006) 1299–1305, http://dx.doi.org/10.1007/s11664-006-0258-y.

[13] D.C. Look, Doping and defects in ZnO, in: C. Jagadish, S.J. Pearton (Eds.), Zinc Oxide Bulk, Thin Films and Nanostructures: Processing, Properties and Applications, Elsevier, Amsterdam, 2006.

[14] J. Zhang, W. Zhang, E. Zhao, H.J. Jacques, Study of high-density AZO ceramic target, Mater. Sci. Semicond. Process. 14 (2011) 189–192, http://dx.doi.org/10.1016/j.mssp.2011.02.004.

[15] G. Fang, D. Li, B.-L. Yao, Fabrication and characterization of transparent conductive ZnO:Al thin films prepared by direct current magnetron sputtering with highly conductive $ZnO(ZnAl_2O_4)$ ceramic target, J. Cryst. Growth 247 (2003) 393–400, http://dx.doi.org/10.1016/S0022-0248(02)02012-2.

[16] H.S. Huang, H.C. Tung, C.H. Chiu, I.T. Hong, R.Z. Chen, J.T. Chang, H.K. Lin, Highly conductive alumina-added ZnO ceramic target prepared by reduction sintering and its effects on the properties of deposited thin films by direct current magnetron sputtering, Thin Solid Films 518 (2010) 6071–6075, http://dx.doi.org/10.1016/J.TSF.2010.06.004.

[17] N. Neves, R. Barros, E. Antunes, J. Calado, E. Fortunato, R. Martins, I. Ferreira, Aluminum doped zinc oxide sputtering targets obtained nanostructures powders: processing and

application, J. Eur. Ceram. Soc. 32 (2012) 4381–4391,
http://dx.doi.org/10.1016/j.jeurceramsoc.2012.08.007.

[18] R.B. Hadj Tahar, Structural and electrical properties of
aluminum-doped zinc oxide films prepared by sol–gel
process, J. Eur. Ceram. Soc. 25 (2005) 3301–3306,
http://dx.doi.org/10.1016/j.jeurceramsoc.2004.08.028.

[19] S. Yang, F. Chen, Q. Shen, L. Zhang, Microstructure and
electrical property of aluminum doped zinc oxide ceramics
by isolating current under spark plasma sintering, J. Eur.
Ceram. Soc. 36 (2016) 1953–1959,
http://dx.doi.org/10.1016/j.jeurceramsoc.2016.02.027.

[20] G.E.P. Box, J.S. Hunter, W.G. Hunter, Statistics for
Experimenters: Design, Innovation and Discovery, John
Wiley & Sons, Inc., Hoboken, NJ, 2005.

[21] M.J. Sánchez-Rivera, A. Gozalbo, V. Pérez-Herranz, S. Mestre,
Experimental design applied to improving the effect of

bismuth oxide as a sintering aid for tin oxide, Bol. Soc. Esp.
Ceram. Vidr. 57 (2018) 119–123,
http://dx.doi.org/10.1016/j.bsecv.2017.10.006.

[22] R.M. German, Sintering Theory and Practice, John Wiley &
Sons, Inc., New York, 1996.

[23] S. Chaturvedi, P.N. Dav, Review on thermal decomposition of
ammonium nitrate, J. Energ. Mater. 31 (2013) 1–26,
http://dx.doi.org/10.1080/07370652.2011.573523.

[24] J. Temuujin, Ts. Jadambaa, K.J.D. Mackenzie, P. Angerer, F.
Porte, F. Riley, Thermal formation of corundum from
aluminium hydroxides prepared from various aluminium
salts, Bull. Mater. Sci. 23 (2000) 301–304.